ORIGINAL PAPER

Scale dependency and anisotropy of mechanical properties of jointed rock masses: insights from a numerical study

Yanyan Li[1] · Rui Wang[1] · Jianping Chen[2] · Zhihong Zhang[1] · Kun Li[3] · Xudong Han[4]

Abstract
Affected by discontinuities, the properties of rock masses are characterized by strong scale dependency and anisotropy. Rock mass samples taken at any scale smaller than the representative elementary volume (REV) size could lead to an incorrect characterization and property upscaling. To better understand the sampling problem, numerical tests based on an outcrop-data-based discrete fracture network (DFN) model were conducted, trying to determine the REV size and its anisotropy. The model was validated and subsequently sampled to produce 455 rectangular samples with a width ranging from 0.05 to 21 m and a constant height-to-width ratio of 2. The samples were introduced into a 3D particle flow code model to create synthetic rock mass (SRM) samples. Numerical uniaxial compressive tests at different loading directions were performed to study the scale dependency and anisotropy of mechanical parameters. The results show that the mechanical REV sizes in different directions differ, changing between 7 and 19 m. The mechanical properties of rock mass samples in a REV size exhibit strong anisotropy, with the values of uniaxial compressive strength (UCS) and elastic modulus (E) varying from 5.6 to 10.3 MPa and 3.9 to 8.0 GPa, respectively. The simulated values of UCS were validated based on GSI and the Hoek–Brown failure criterion. The geometrical REV size based on the volumetric fracture intensity was calculated to be 7 m, equal to the minimum of the mechanical REV size; this suggests that the geometrical REV defines the lower bound of the REV size.

Keywords Anisotropy · Scale dependency · Representative elementary volume · Fracture network model · Synthetic rock mass

Introduction

The mechanical properties of rock masses and their anisotropy are critical for the design of engineering structures, such as radioactive waste disposal, deep-buried tunnels, and hydropower dams. Affected by geological discontinuities, the properties of rock masses are characterized by strong scale dependency and anisotropy (Bieniawski 1968;

✉ Yanyan Li
lee_xandy@126.com

1 Faculty of Urban Construction, Beijing University of Technology, Beijing 100124, China

2 College of Construction Engineering, Jilin University, Changchun 130026, China

3 General Institute of Water Resources and Hydropower Planning and Design, Ministry of Water Resources, Beijing 100120, China

4 Center For Hydrogeology and Environmental Geology, China Geological Survey, Baoding 071051, China

Oda 1983; Cho et al. 2012; Park and Min 2015; Wu et al. 2020; Zheng et al. 2020). The strength, deformability, and permeability parameters obtained from rock samples in the laboratory rarely represent the parameters of rock masses at the engineering scale (Hudson and Harrison 1997; Wu and Kulatilake 2012; Khani et al. 2013). Although in situ tests provide an insight into the mechanical behaviors of rock masses under loading, they are expensive, time-consuming, and have uncertainty in determining whether the size of the influenced zone is large enough to represent the overall rock mass (Bieniawski 1973; Oda 1988). Therefore, it is still a challenge to obtain effective mechanical properties of rock masses for engineering purpose.

The representative elementary volume (REV), defined as the minimum volume beyond which the tested rock samples behave like the whole rock mass (Bear 1972; Oda 1988), provides a way to quantify the size-dependent property of the mechanical properties (Esmaieli et al. 2010). It determines whether a jointed rock mass could be treated as an equivalent continuum since there is no guarantee that a REV always

exists (Long et al. 1982; Min et al. 2004; Azizmohammadi and Matthäi 2017).

Numerous studies on REV have been conducted in the past to quantify the size of REV. To date, the parameters used to determine the REV size can be grouped into three board categories: (1) hydraulic parameters (Oda 1982, 1988; Long 1982; Wang et al. 2002; Min et al. 2004; Azizmohammadi and Matthäi 2017), (2) geometrical parameters (Hudson and Harrison 1997; Li et al. 2018), and (3) mechanical parameters (Min and Jing 2003; Wu and Kulatilake 2012). A variety of hydraulic parameters are used to determine the existence of REV, such as block permeability (Kulatilake and Panda 2000), hydraulic conductivity (Wang et al. 2002), and permeability tensor (Min et al. 2004; Chen et al. 2008; Zou et al. 2018). The REV size is also considered a function of geometrical parameters of fractures, such as fracture spacing (Pariseau et al. 2008), fracture intensity (Esmaieli et al. 2010; Zhang et al. 2012; Ni et al. 2017), blockiness (Xia et al. 2016), and fracture connectivity (Li et al. 2018). For example, Pariseau et al. (2008) and Xia et al. (2016) indicated that the REV size is 2 to 20 times fracture spacing. The mechanical parameters used to quantify the REV size mainly include uniaxial compressive strength (UCS), elastic modulus, Poisson's ratio, and shear modulus. For example, Min and Jing (2003) and Khani et al. (2013) determined the REV size of rock masses using the elastic modulus and Poisson's ratio. Esmaieli et al. (2010) and Laghaei et al. (2018) utilized elastic modulus and UCS to estimate the REV size based on a series of numerical uniaxial compressive tests. Wang et al. (2017) studied scale effects, REV, and anisotropic properties of rock masses using shear stress obtained by numerical direct shear tests. Wu et al. (2019) obtained the REV size of the rock mass in the Xiaowan hydropower station based on UCS. Huang et al. (2020) proposed a method combining the PFC-based synthetic rock mass model with the Hoek–Brown failure criterion to determine the REV size using UCS, elastic modulus, and geological strength index (GSI) and found that the GSI-based indicator yielded relatively larger REV size compared with traditional UCS or deformation modulus-based indicators.

The following limitations should be considered in the estimation of the REV size:

1. Since geometrical parameters only provide information on structural characteristics of a rock mass, they cannot wholly reflect the mechanical behaviors, and thus, they can only be used for initial estimation of the REV size in a time-efficient manner (Ni et al. 2017; Huang et al. 2020);

2. Hydraulic parameters are mainly derived from two-dimensional networks, which inevitably underestimate the connectivity and permeability of three-dimensional networks (Lang et al. 2014); and

3. The mechanical properties of rock mass are characterized by strong anisotropy. Accordingly, the REV sizes in different directions vary attributed to the anisotropy (Wang et al. 2017; Wu et al. 2019), which has not been considered by previous work when estimating the REV size.

The Songta dam, located on the upstream of the Nu River in southwest China, is designed to be a double-curved arch dam with a maximum height of 318 m (Li et al. 2014). The determination of rock mass strength and deformation properties is important in evaluating the rock mass stability at the dam site. This paper presents an investigation on the scale dependency and anisotropy of mechanical properties of the rock mass. A three-dimensional (3D) discrete fracture network (DFN) model was built based on joint data collected from an exploration tunnel at the dam site. The model was validated and subsequently sampled to procure 455 rectangular specimens with a width ranging from 0.05 to 21 m and a constant height-to-width ratio of 2. The specimens were introduced into a 3D particle flow code (PFC3D) model to create synthetic rock mass (SRM) samples. Numerical uniaxial compressive tests with different loading directions were conducted to obtain the UCS and elastic modulus of the SRM samples. The REV size of the rock mass was finally determined.

Generation of a fracture system model

Data collection

Fracture mapping was conducted in an excavation tunnel at the Songta dam site on the upstream of Nu River in southwest China. The lithology is mainly composed of Cretaceous biotite granite. Besides, mafic intrusive rocks outcrop as dykes with width ranging from 0.05 to 5 m (Li et al. 2017). The tunnel is 200 m long, 2 m wide, and 2 m high, with a strike of E-W. According to the unloading and weathering degree, the rock mass along the tunnel is divided into three zones: strongly disturbed zone, weakly disturbed zone, and undisturbed zone (Han et al. 2016). A total of 128 joints were collected from a relatively homogeneous area with a length of 80 m using the window sampling method (Wu and Pollard 1995; Mauldon et al. 2001; Manda and Mabee 2010; Li et al. 2014) (Fig. 1a): all the joints that intersect the south-side wall of the tunnel, with trace length longer than 0.5 m, were mapped. The joints were grouped into three sets using the fuzzy K-means algorithm (Hammah and Curran 1999), as shown in Fig. 1b: (1) set 1 composed of joints with shallow dip angles, (2) set 2 composed of steeply dipping joints, and (3) set 3 composed of moderately dipping joints.

(a)

(b)
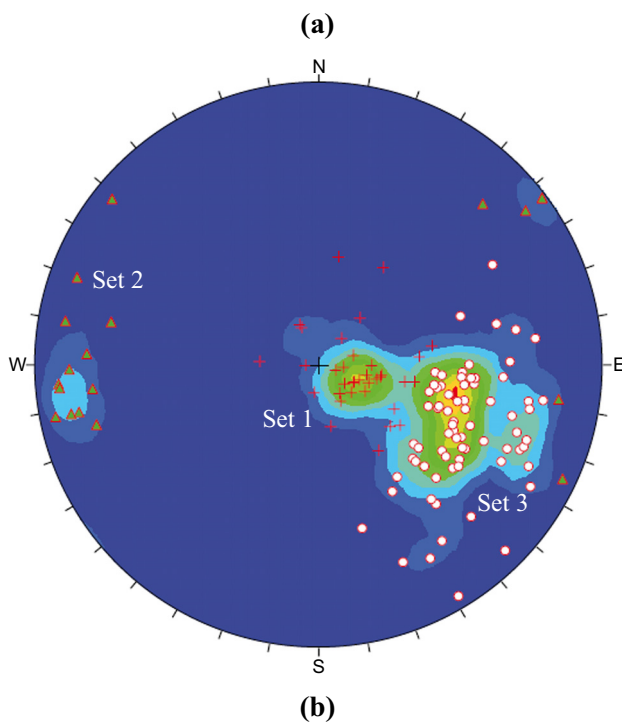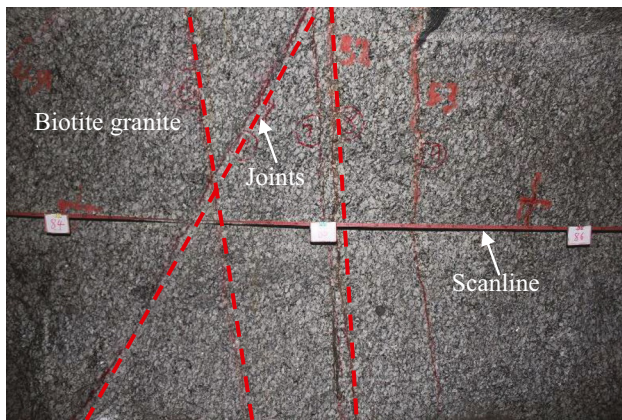
Fig. 1 **a** Fracture mapping in a tunnel using the window sampling method. **b** Upper-hemisphere and equal-area projections of 128 joint orientations obtained from a relatively homogeneous area with a length of 80 m in the undisturbed zone. The joints were grouped into three sets: set 1 composed of joints with shallow dip angles, set 2 composed of steeply dipping joints, and set 3 composed of moderately dipping joints

Estimation of UCS using GSI

The UCS of rock mass (σ_{cm}) is estimated using the Hoek–Brown failure criterion and the geological strength index (GSI) (Hoek and Brown 1997; Marinos and Hoek 2000):

$$\sigma_{cm} = \sigma_c s^{0.5} \tag{1}$$

$$s = \exp\frac{(GSI - 100)}{9} \tag{2}$$

where σ_c is the UCS of intact rock mass which is equal to 127.0 MPa in this work (Zhao and Huang 2018), and s is rock mass strength characteristic parameters. The value of GSI varies between 45 and 55 based on geological conditions and rock types. According to Eqs. (1) and (2), the value of σ_{cm} varies from 6.0 to 10.4 MPa.

Fracture network modeling

The three-dimensional discrete fracture network (DFN) model used in this work was built by our previous research (Han et al. (2016)). The distribution types of joint geometry parameters were obtained using statistical analysis. The parameters used for establishing the DFN model are listed in Table 1 (Han et al. 2016). To build a 3D DFN model, the statistical distributions for (1) the location of fracture centers, (2) orientation, and (3) diameter (Kulatilake et al. 2003) should be determined. In this work, the geometry of a joint was considered a disk with the center following a homogeneous Poisson distribution (Kulatilake et al. 2003; Min et al. 2004; Hardebol et al. 2015; Han et al. 2016). Joint orientations were assumed to follow empirical distributions (Oda 1982; Kulatilake et al. 1993). The joint diameter can be estimated based on the trace length distribution using the stereological method (Warburton 1980; Zhang and Einstein 1998). If the trace length has a lognormal distribution with mean μ_L and standard deviation σ_L, the mean diameter μ_D is calculated by the following (Zhang and Einstein 1998, 2000):

Table 1 Fracture modelling parameters for the study region (Han et al. 2016)

Joint set	Joint number	Dip direction (°)	Dip (°)	Fisher constant	Measured trace length			Joint size		Joint density (m⁻³)
					Mean (m)	Std. (m)	Distribution	Mean (m)	Std. (m)	
1	35	100.6	11.8	28.40	2.19	1.57	Gamma	2.02	1.65	0.160
2	19	265.0	82.2	10.87	1.48	0.57	Lognormal	3.55	0.90	0.030
3	74	113.3	48.3	17.11	1.35	0.79	Lognormal	3.86	1.89	0.062

Fig. 2 3D DFN model (*red lines* joint set 1, *blue lines* joint set 2, *green lines* joint set 3). In the model, the *x*-direction refers to the west, and the *y*-direction refers to the south
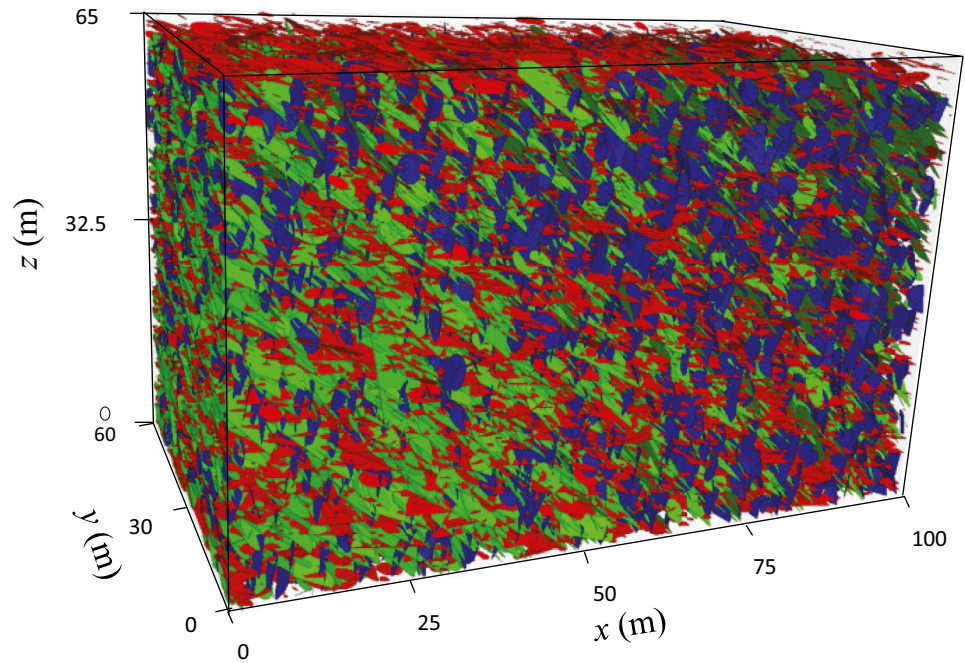
$$\mu_D = \frac{128(\mu_L)^3}{3\pi^3[(\mu_L)^2 + (\sigma_L)^2]} \tag{3}$$

If the trace length follows a Gamma distribution, μ_D is obtained by the following (Zhang and Einstein 1998, 2000):

$$\mu_D = \frac{64(\mu_L)^2 - 3\pi^2[(\mu_L)^2 + (\sigma_L)^2]}{8\pi\mu_L} \tag{4}$$

The volume density λ_i^V can be estimated using the normal linear density λ_i^1 (Oda 1982; Kulatilake et al. 1993; Zhang and Einstein 2000).

$$\lambda_i^V = \frac{4\lambda_i^1}{\pi E(D^2)} \tag{5}$$

where $E(D^2)$ is the second moment of the joint diameter distribution.

The size of the 3D DFN model was set as 100 m $\times$ 60 m $\times$ 60 m. The Monte-Carlo method was used to simulate the location, orientation, and size of joints according to their statistical parameters using a Poisson process (Chen et al. 1995; Hardebol et al. 2015). Finally, a 3D DFN model was established by combining the three geometry parameters into one model (Fig. 2). The model was verified by comparing joint data measured in the tunnel with the simulated joint data obtained from an artificial sampling window in the DFN model which has the same size and location as the field sampling plane. The compared parameters include the number of joints, mean dip direction, mean dip angle, mean trace length, and spherical standard deviation, as listed in Table 2. Table 2 shows that the simulated joint data agree well with the field data.

Synthetic rock mass models

In this study, a series of numerical simulations using the 3D particle flow code (PFC3D) were carried out. A synthetic rock mass (SRM) technology was used to simulate jointed rock masses. In SRM, rock matrix is represented as

Table 2 Comparison between the field data and the simulated data obtained from the DFN model

Joint set		Joint number	Dip direction (°)	Dip (°)	Trace length (m)	Spherical Std. (°)
1	Field	35	100.6	11.8	2.19	8.75
	Simulated	34	89.8	8	2.47	9.88
2	Field	19	265	82	1.48	14.43
	Simulated	20	272.5	79	1.26	13.08
3	Field	74	113.3	48.3	1.35	10.01
	Simulated	73	112.1	45.3	1.65	9.85

(a) BPM simulation of intact rock   **(b)** SRM   **(c)** SJM simulation of discontinuities
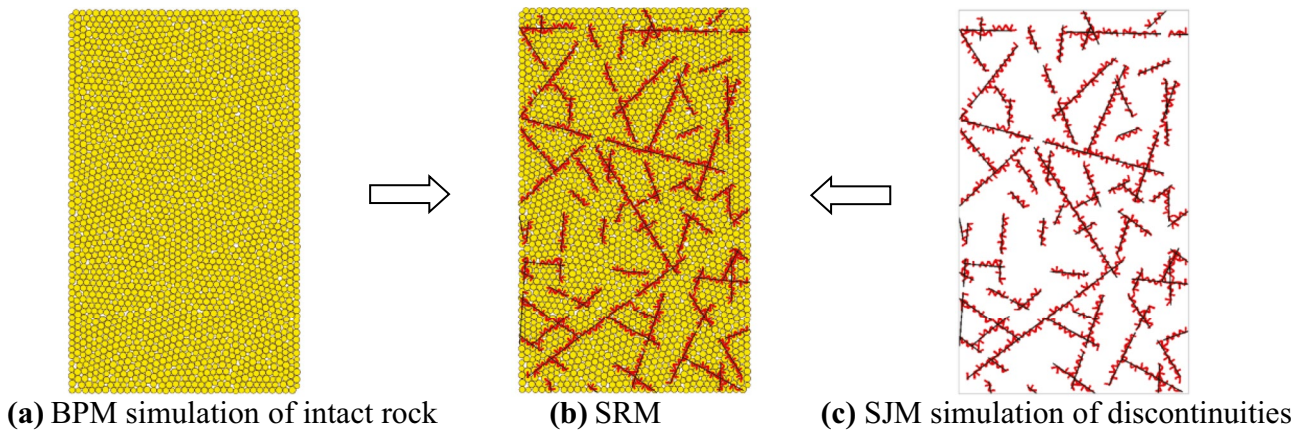
Fig. 3 Schematic diagram of the SRM model, where BPM and SJM are used to represent intact rock and discontinuities, respectively
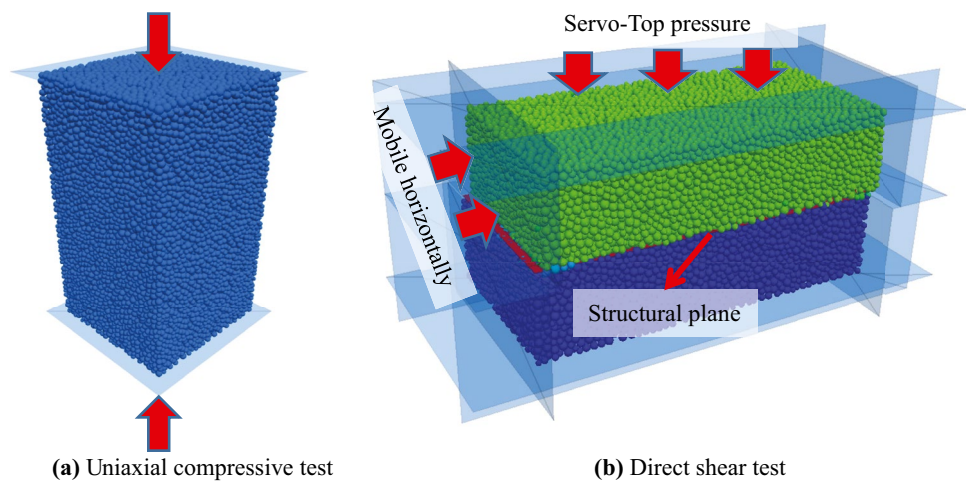
an assembly of bonded particles using the bonded particle model (BPM) (Potyondy and Cundall 2004), and discontinuities are simulated by the smooth joint model (SJM) (Ivars et al. 2008, 2011). The SRM model is established by integrating a DFN within PFC3D particle assembly. Figure 3 shows the main components of a SRM sample.

Micro-parameters of the bonded particle model for intact rocks

PFC3D simulates rock matrix and discontinuities by assigning microscopic parameters to particles and contact models, rather than directly using mechanical parameters obtained from laboratory tests. The contact model between particles in BPM for intact rocks is the parallel bond model (PBM). The micro-parameters of the PBM and SJM need to be calibrated to fit the laboratory properties in a trial-and-error manner (Potyondy and Cundall 2004; Bastola et al. 2020).

In this research, calibration of the micro-parameters of intact rock models was carried out by performing a series of uniaxial compressive tests (Fig. 4a) and comparing the simulation results with the laboratory test results. The wall-based loading procedure in PFC3D (Esmaieli et al. 2010) with a displacement rate of 0.15 m/s was applied on 13 intact rock models with a constant height-width ratio of 2 and width ranging from 0.05 m to 21 m (i.e., 0.05, 0.5, 1, 3, 5, …, 21 m). It is assumed that the strength of the intact rock samples with different sizes remains constant. The target values of uniaxial compressive strength (UCS), elastic modulus (E), and Poisson's ratio (v) of the intact rock models with different sizes are 127.0 MPa, 38.7 GPa, and 0.15, respectively (Zhao and Huang 2018). Poisson's ratio v was obtained by calibrating the normal-to-shear stiffness ratio k_n/k_s, the effective modulus E was modified to acquire the target elastic modulus, and the uniaxial compressive strength (UCS) was obtained by calibrating bond tensile strength and

Fig. 4 Numerical tests used in the calibration

Servo-Top pressure

Mobile horizontally

Structural plane

(a) Uniaxial compressive test   **(b)** Direct shear test

Table 3 Micro-parameters of the BPM models

Sample size (m)	ρ (kg/m^3)	Rmin (m)	Rmax/Rmin	Porosity	μ	$\overline{E}c$ (GPa)	$\overline{k}n$ /$\overline{k}s$	$\overline{\sigma}_c$(MPa)	$\overline{c}$ (MPa)	$\overline{\varphi}$ (°)
0.05	2670	0.00075	1.66	0.35	0.5	34	1.1	70	130	50
0.5	2670	0.0075	1.66	0.35	0.5	34	1.1	70	130	50
1	2670	0.015	1.66	0.35	0.5	34	1.1	70	130	50
3	2670	0.045	1.66	0.35	0.5	34	1.1	70	130	50
5	2670	0.075	1.66	0.35	0.5	34	1.1	70	130	50
7	2670	0.105	1.66	0.35	0.5	34	1.1	70	130	50
9	2670	0.135	1.66	0.35	0.5	34	1.1	70	130	50
11	2670	0.165	1.66	0.35	0.5	34	1.1	70	130	50
13	2670	0.195	1.66	0.35	0.5	34	1.1	70	130	50
15	2670	0.225	1.66	0.35	0.5	34	1.1	70	130	50
17	2670	0.255	1.66	0.35	0.5	34	1.1	70	130	50
19	2670	0.285	1.66	0.35	0.5	34	1.1	70	130	50
21	2670	0.315	1.66	0.35	0.5	34	1.1	70	130	50

ρ density, *Rmin* minimum particle radius, *Rmax* maximum particle radius, μ friction coefficient of particles, $\overline{E}c$ parallel bond modulus, $\overline{k}n$ / $\overline{k}n$ parallel bond normal-to-shear stiffness ratio, $\overline{\sigma}_c$ parallel bond tensile strength, $\overline{c}$ parallel bond cohesion, $\overline{\varphi}$ parallel bond friction angle

Table 4 Mechanical properties calculated from the intact rock models

Sample size (m)	UCS (MPa)	E (GPa)	v
0.05	130.8	38.3	0.15
0.5	125.1	38.2	0.15
1	131.2	38.2	0.15
3	131.8	38.4	0.15
5	127.8	38.2	0.15
7	127.3	38.4	0.15
9	126.0	38.3	0.15
11	125.9	38.7	0.15
13	126.0	38.3	0.15
15	126.5	38.4	0.15
17	126.6	38.3	0.15
19	125.3	38.4	0.15
21	127.9	38.3	0.15

bond cohesion. The particle properties were calibrated until comparable macroscopic rock properties are achieved. The micro-properties of particles and PBM are listed in Table 3,

respectively. The intact rock models with different sizes were calibrated to UCS of 125.1 to 131.2 MPa, E of 38.2 to 38.7 GPa, and v of 0.15 (Table 4).

Micro-parameters of the smooth joint model for fractures

In the study area, the properties of joints in different sets vary. Joints of set 1 have shallow dip angles and are mainly filled by rock debris and mud, whereas most of joints in sets 2 and 3 have no filling. According to previous work conducted by Zhao and Huang (2018), the friction coefficient of joints in set 1 ranges from 0.35–0.45, and the friction coefficient of joints in sets 2 and 3 ranges from 0.45–0.70. Besides, all joints in the model are assumed to be cohesionless (Zhang et al. 2015).

The smooth joint model (SJM) was used to simulate the behavior of a planar interface. The model has three input microparameters: normal stiffness, shear stiffness, and friction coefficient. As shown in Fig. 4b, the direct shear test was conducted to calibrate the microscopic parameters of SJM. The velocities of the sidewalls were adjusted using

Fig. 5 Shear stress–shear displacement graphs at different normal stresses


(a) Joints of set 1

(b) Joints of sets 2 and 3
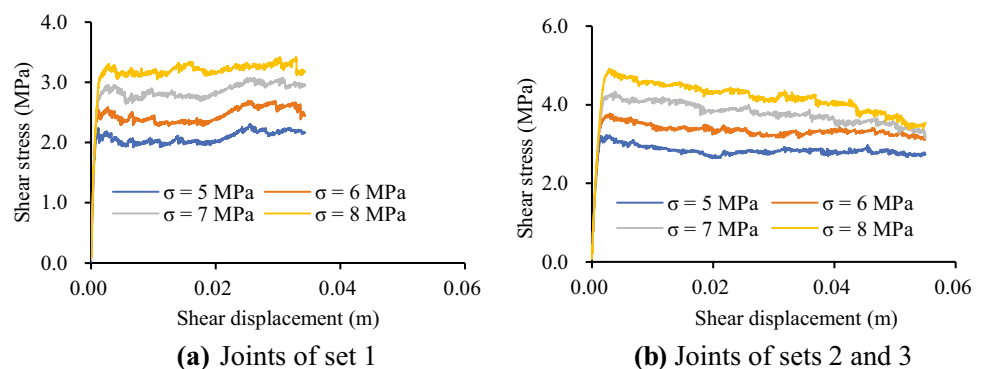
Table 5 Calibrated micro-parameters for SJM

SJM parameters	Set 1	Sets 2 and 3
Normal stiffness per unit area (Gpa/m)	15	15
Shear stiffness per unit area (Gpa/m)	9	9
Friction coefficient	0.4	0.65
Tensile strength (MPa)	0	0
Cohesion (MPa)	0	0

a servo-control mechanism so that a target pressure was applied to the top of the model. The lower sidewalls were immobile and the upper sidewalls were moved horizontally with a fixed speed to apply the shear stress. The loading velocity in the direct shear test is 0.1 m/s.

Bahaaddini et al. (2013, 2015, and 2016) found the particle interlocking during the 2D modeling of the joint direct shear tes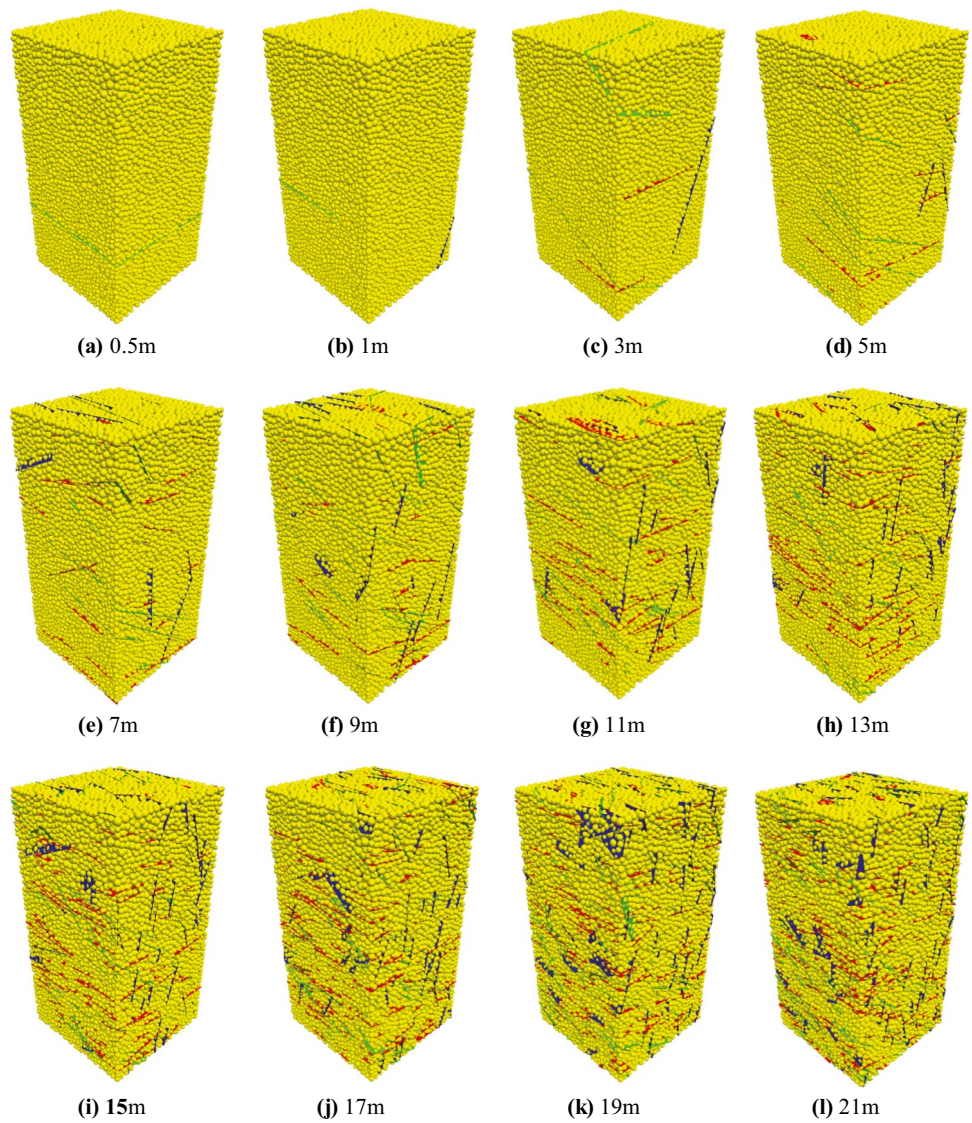t. When the shear displacement of the joint exceeds the minimum particle diameter, the shear stress suddenly increases and leads to an unrealistic dilation of rock joints. However, Mehranpour and Kulatilake (2017) found that this behavior was not obvious in the 3D modeling of the joint direct shear test. Lower normal stiffness, higher joint normal stiffness, higher ratio of the particle size to the shear displacement, and higher ratio of the particle size to the joint length can bring down the number of interlocking incidents to as low as zero (Mehranpour and and Kulatilake 2017). This work used the method proposed by Mehranpour and and Kulatilake (2017) to solve the interlocking problem in the simulations. As shown in Fig. 5, no obvious abrupt increase in the shear stress was observed in the direct shear test for different kinds of joints. However, there are shear stress drops during the shearing process, especially for joints in sets 2 and 3 (Fig. 5b). This is because the shear stress was calculated according to the shear forces acting on the smooth-joint contacts, and the shear force acting on the non-smooth joint was ignored.

Fig. 6 Rock mass samples with different sizes extracted from the 3D DFN model

(a) 0.5m   (b) 1m   (c) 3m   (d) 5m

(e) 7m   (f) 9m   (g) 11m   (h) 13m

(i) 15m   (j) 17m   (k) 19m   (l) 21m
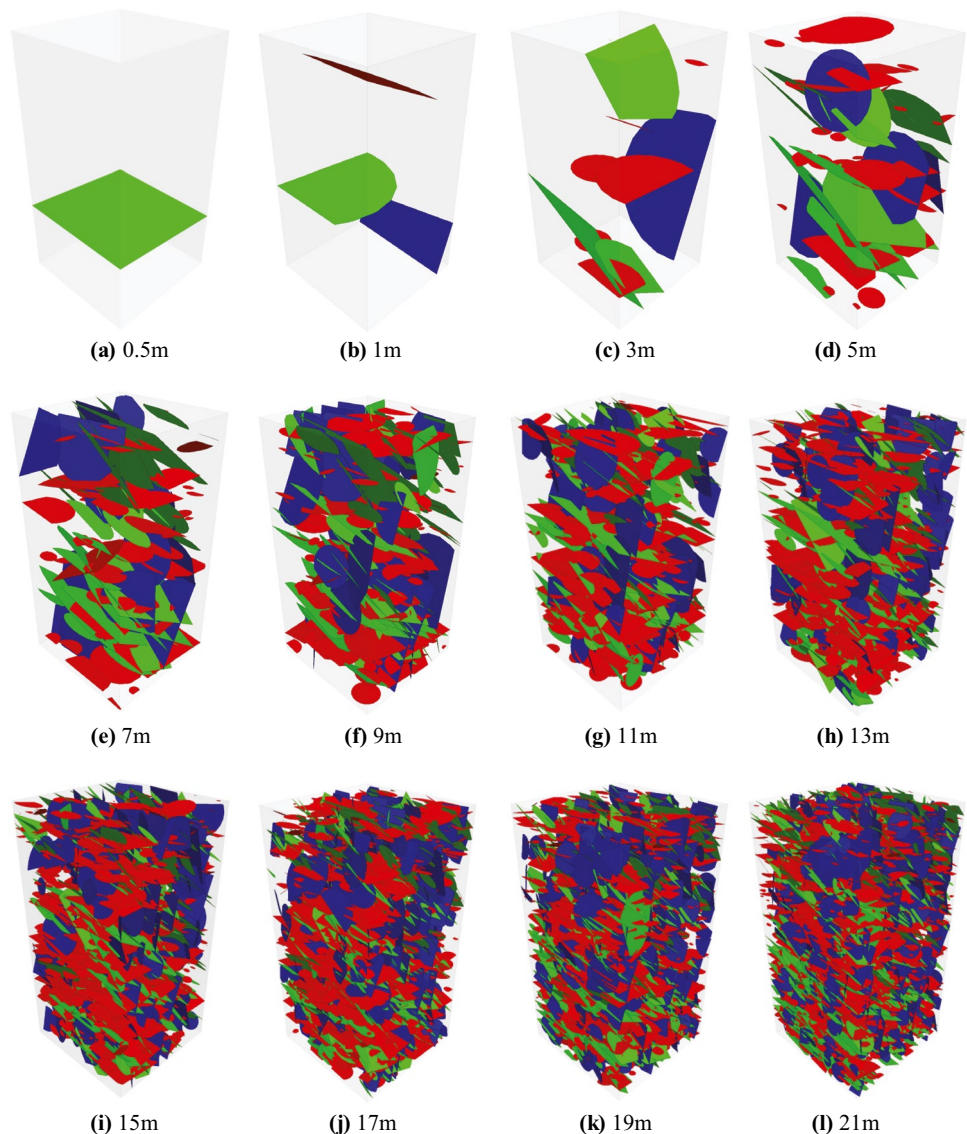
Fig. 7 Synthetic rock mass (SRM) samples with different sizes

(a) 0.5m   (b) 1m   (c) 3m   (d) 5m

(e) 7m   (f) 9m   (g) 11m   (h) 13m

(i) 15m   (j) 17m   (k) 19m   (l) 21m

The value of SJ normal stiffness and SJ shear stiffness was determined by previous studies (Bahaaddini et al. 2013, 2015 and 2016; Mehranpour and and Kulatilake 2017), and trial–error direct shear tests were used to acquire the target friction coefficient. The micro-mechanical properties of SJM are listed in Table 5. The values of the calibrated friction coefficient of joints in set 1, and joints in sets 2 and 3 are 0.40 and 0.61, respectively, which are close to the target values.

Fig. 8 Variation of **a** UCS and **b** E with rock sample sizes under vertical loading

(a)   (b)
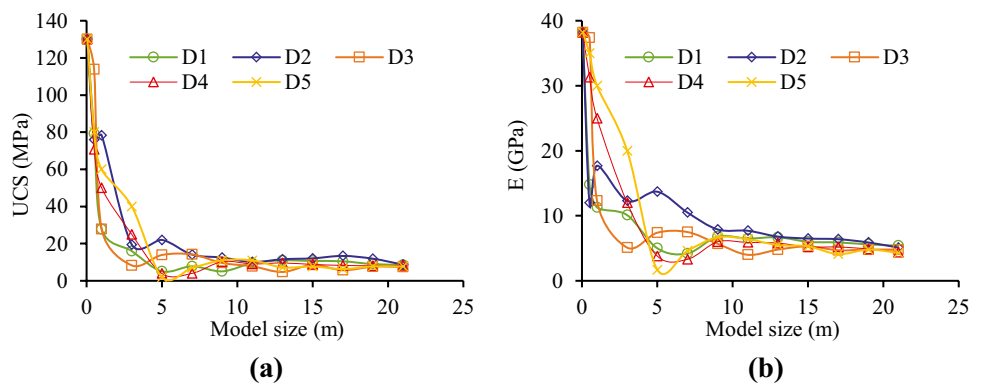
**Table 6** CV results for estimating REV size based on uniaxial compression tests under vertical loading

Sample ID	Sample size (m)	CV of UCS	CV of E
a	0.5	0.20	0.45
b	1	0.44	0.42
c	3	0.55	0.45
d	5	0.90	0.73
e	7	0.48	0.49
f	9	0.29	0.13
g	11	0.13	0.22
h	13	0.32	0.14
i	15	0.19	0.10
j	17	0.36	0.17
k	19	0.19	0.10
l	21	0.07	0.10

These optimal values of input micro-parameters could give proper macro-properties of the fracture.

Results and discussions

Scale dependency of mechanical properties of the rock mass under vertical loading

Following traditional guidelines (Esmaieli et al. 2010; Laghaei et al. 2018; Wu et al. 2019; Huang et al. 2020), the loading direction in uniaxial compressive tests is firstly set
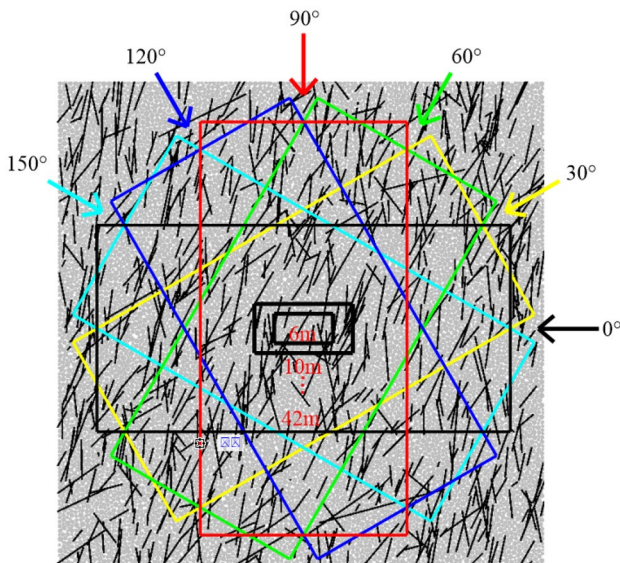
Fig. 9 Schematic diagram of six loading directions used in uniaxial compression tests to study the anisotropy of the rock mass. Note that the rotational angle θ ($\theta = 0°$, $30°$, …, $150°$) in the counter-clockwise direction is the included angle between the loading direction and the x-direction

as vertical, which is parallel to the z-direction. Thirteen cubic BPM models with a constant height-width ratio of 2 and with width ranging from 0.05 m to 21 m (i.e., 0.05, 0.5, 1, 3, 5, …, 21 m) were established. Five DFN models with the centroids of D_1 (30 m, 30 m, 30 m), D_2 (40 m, 30 m, 30 m), D_3 (50 m, 30 m, 30 m), D_4 (60 m, 30 m, 30 m), and D_5 (70 m, 30 m, 30 m) were extracted from the "master" DFN model with the size of 100 m × 60 m × 60 m, respectively, and the size of each selected DFN model is 27 m × 27 m × 54 m. In all, 65 SRM models were established by integrating each DFN model within each BPM model assembly. The distributions of fractures in the rock mass models with different sizes are shown in Fig. 6. Note that the sample with a width of 0.05 m is not shown in Fig. 6 since it has no crack. The SRM samples generated by PFC3D are shown in Fig. 7.
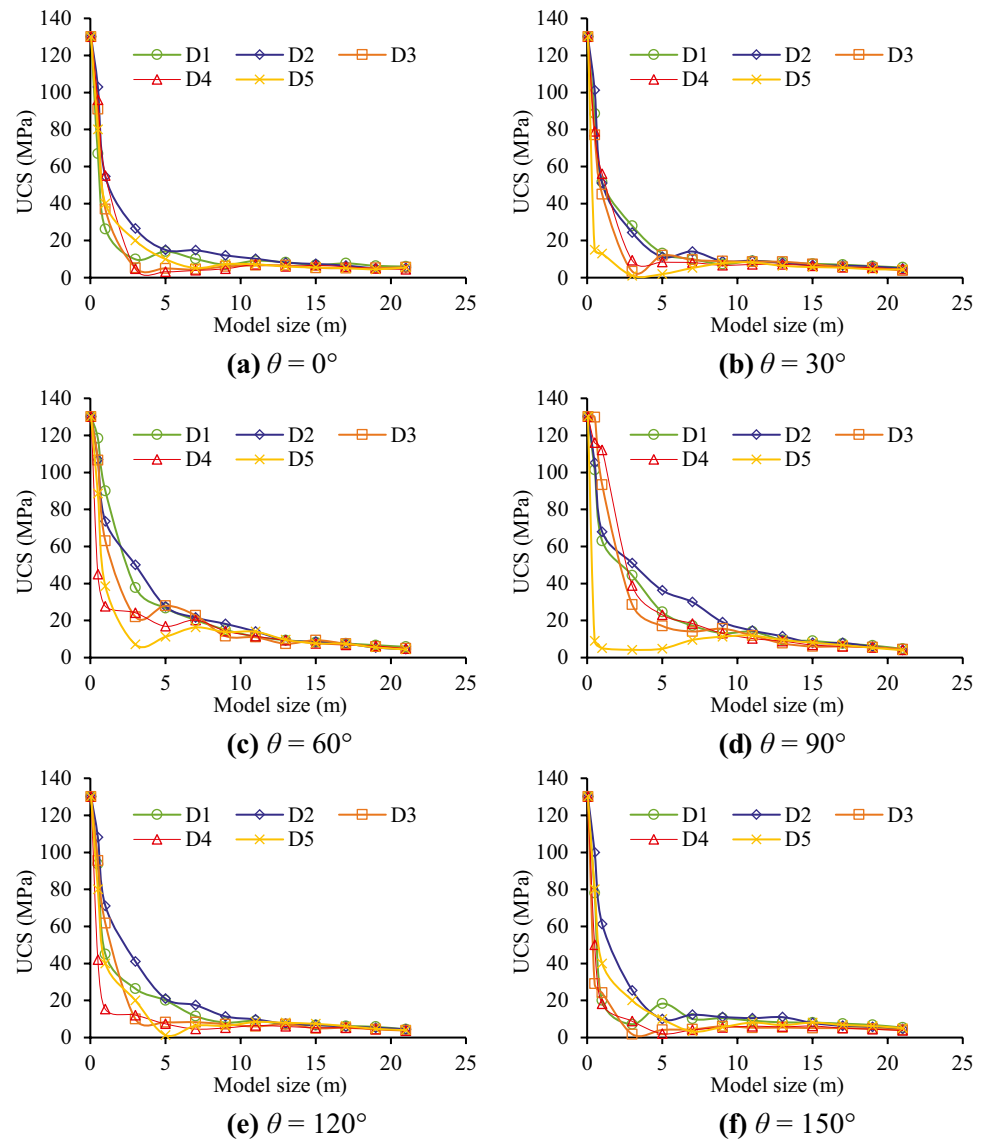
A series of uniaxial compressive tests under vertical loading were conducted to investigate the variation of mechanical properties with sample sizes. The loading velocity is 0.15 m/s. Figure 8a shows that the values of UCS for samples in different regions fluctuate dramatically when the sample size varies from 0.05 to 7 m, but decreases gradually to a stable value with increasing scales. In this study, the average modulus was selected as the elastic modulus. Figure 8b shows that the values of E change remarkably when the sample size is less than 12 m. When the model size increases to 13 m, the value of E tends to stabilize.

The coefficient of variance (C_V), defined as the ratio of the standard deviation to the mean value, was used to determine the REV size of the rock mass. C_V represents the variations when the average of data remains constant and is widely used to determine the REV size of rock masses by previous studies (Baghbanan 2008; Esmaieli et al. 2010; Laghaei et al. 2018; Huang et al. 2020). According to Baghbanan (2008), Laghaei et al. (2018), and Huang et al. (2020), a sample size could be regarded as REV when the value of C_V is less than 0.2. The results (Table 6) show that the C_V values of UCS are less than 0.2 when the sample size reaches 19 m. However, the C_V values of E are less than 0.2 when the sample size reaches 13 m. Therefore, the UCS-based and E-based REV sizes in the vertical direction are 19 m and 13 m, respectively. It is determined that the mechanical REV size in the vertical direction is 19 m by integrating UCS and E. The values of UCS and E in the REV size are 8.8 MPa and 5.0 GPa, respectively. Compared with the values of UCS (127 MPa) and E (38.7 GP) of intact rock, the values of UCS and E of the rock mass in the vertical direction are relatively decreased by 93.1% and 87.1%, respectively.

Scale dependency and anisotropy of mechanical properties of the rock mass under horizontal loading

The abutment, designed to support the arch dam, is located in this area. The rock mass mainly suffers from the

Fig. 10 Variation of the values of UCS with rock sample sizes in different loading directions

(a) $\theta = 0°$

(b) $\theta = 30°$

(c) $\theta = 60°$

(d) $\theta = 90°$

(e) $\theta = 120°$

(f) $\theta = 150°$

horizontal load from the concrete arch (Lyu et al. 2021). Therefore, the mechanical properties of the rock mass in the horizontal direction will strongly influence the safety of the dam. In this section, uniaxial compressive tests under different loading directions within the horizontal plane (*x*–*y* plane) were carried out to study the anisotropy of mechanical properties of the rock mass. For each model, six rotational angles θ ($\theta = 0°$, 30°, …, 150°) in the counter-clockwise direction (Fig. 9), where θ is the included angle between the loading direction and the *x*-direction, were selected. For each loading direction, 65 models with a height-width ratio of 2 and width ranging from 0.05 to 21 m (0.05, 0.5, 1, 3, 5, …, 21 m) were sampled from the five regions. In all, 390 models were sampled from the 100 m × 60 m × 60 m model.

The results (Figs. 10 and 11) show that the variation trends of UCS and *E* are similar in different loading

directions. For each rotational angle, the values of UCS and *E* for samples in different regions fluctuate dramatically when the sample size is small, but tend to be stable with increasing sizes.

The C_V values of UCS and *E* when the rotational angle varies from 0 to 150° with an interval of 30° are listed in Table 7. The results show that the UCS-based indicator provides similar results with the *E*-based indicator. For rational angles of 0°, 30°, 60°, 90°, and 120°, the results provided by the UCS-based indicator agree well with the *E*-based indicator. Both indicators indicate that the mechanical REV sizes for $\theta = 0°$, 30°, 60°, and 90° are 11 m, 9 m, 7 m, and 11 m, respectively. For $\theta = 120°$, the C_V values of UCS are almost all lower than 0.20 when the sample size is larger than 13 m, and the C_V values of *E* are less than 0.20 when the sample size is larger than 11 m. For $\theta = 150°$, the C_V values of

Fig. 11 Relationships between elastic modulus (*E*) and rock sample sizes in different loading directions

(a) $\theta = 0°$

(b) $\theta = 30°$

(c) $\theta = 60°$

(d) $\theta = 90°$

(e) $\theta = 120°$

(f) $\theta = 150°$
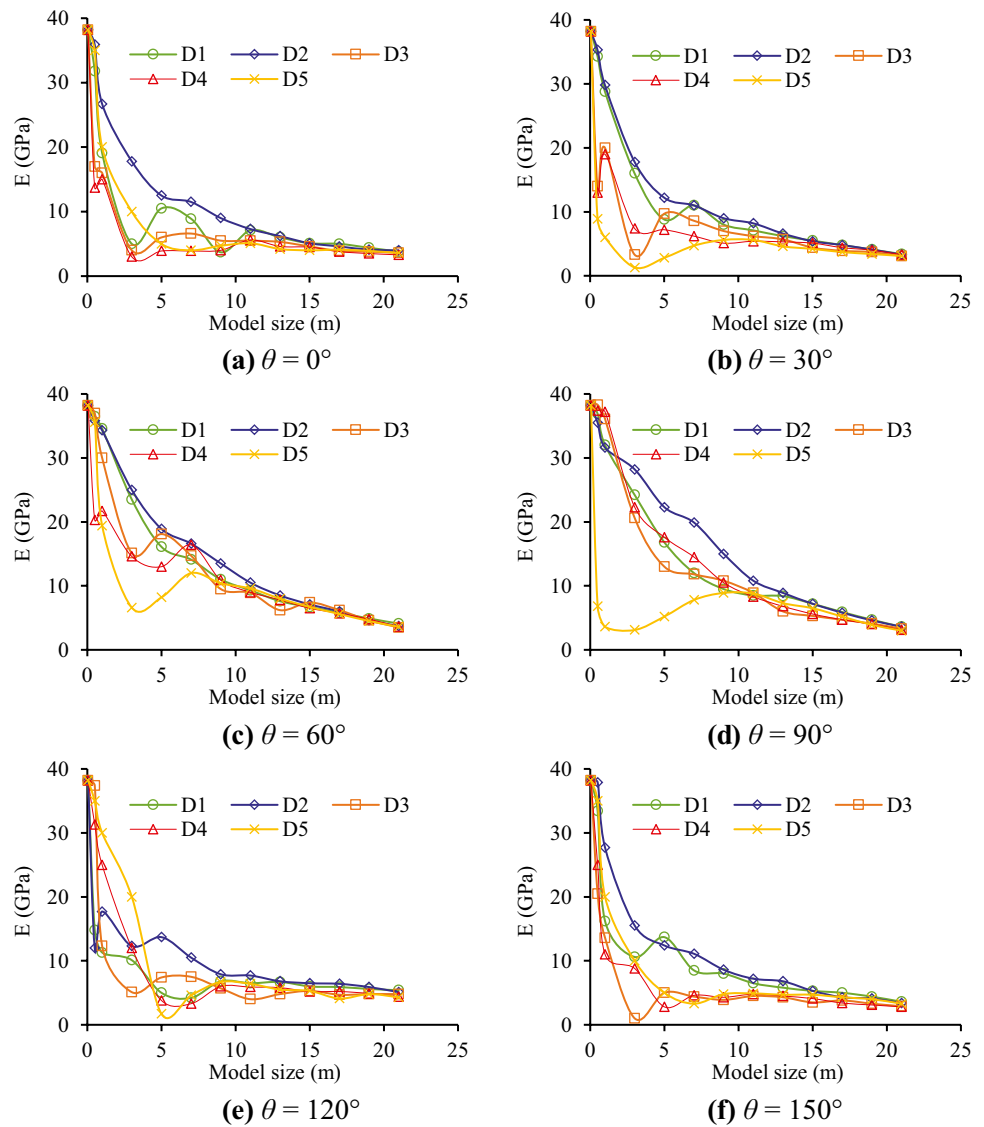
UCS are almost all lower than 0.20 when the sample size is larger than 15 m, and the C_V values of *E* are less than 0.20 when the sample size is larger than 13 m. Therefore, it is comprehensively determined that the mechanical REV size for $\theta = 120°$ and $\theta = 150°$ are 13 m and 15 m, respectively. The results show that the mechanical REV sizes in different directions differ, exhibiting strong anisotropy (Fig. 12). The REV size for $\theta = 60°$ is the minimum, whereas the REV size for $\theta = 150°$ is the maximum.

Affected by discontinuities, the mechanical parameters of rock mass samples in a REV size exhibit strong anisotropy in the six loading directions (Fig. 13). Figure 13 shows that the maximum value of UCS (10.3 MPa) and *E* (8.0 GPa) occurred when θ is 60°, and the minimum value of UCS (5.6 MPa) and *E* (3.9 GPa) was obtained when θ is 150°. It seems that the mechanical properties of the rock mass

for $\theta = 150°$ is the weakest, whereas $\theta = 60°$ is the strongest direction for the mechanical properties. According to Figs. 12 and 13, the mechanical properties of rock mass samples for $\theta = 60°$ is the maximum, whereas the REV size in this direction is the minimum. Besides, the mechanical properties of rock mass samples for $\theta = 150°$ is the minimum, but the REV size in this direction is the maximum. Therefore, it could be concluded that the REV size has a negative relationship with the mechanical properties of the rock mass.

Comparison between mechanical REV and geometrical REV

In this work, the volumetric fracture intensity, represented by the number of fractures per unit volume (P_{30}) and the fracture

Table 7 CV results for estimating REV size based on UCS and E with different loading directions within the x-y plane

| Sample ID	Sample size (m)	$\theta=0°$		$\theta=30°$		$\theta=60°$		$\theta=90°$		$\theta=120°$		$\theta=150°$	
		CV of UCS	CV of E	CV of UCS	CV of E	CV of UCS	CV of E	CV of UCS	CV of E	CV of UCS	CV of E	CV of UCS	CV of E
a	0.5	0.16	0.39	0.46	0.60	0.31	0.22	0.52	0.44	0.30	0.19	0.41	0.24
b	1	0.29	0.24	0.40	0.46	0.43	0.25	0.59	0.50	0.46	0.34	0.56	0.37
c	3	0.72	0.77	0.93	0.81	0.58	0.44	0.55	0.49	0.57	0.49	0.77	0.57
d	5	0.56	0.49	0.48	0.43	0.35	0.29	0.54	0.43	0.74	0.64	0.71	0.63
e	7	0.61	0.47	0.34	0.34	0.12	0.13	0.43	0.34	0.53	0.54	0.60	0.52
f	9	0.37	0.40	0.12	0.23	0.16	0.13	0.21	0.22	0.31	0.28	0.36	0.37
g	11	0.19	0.16	0.10	0.18	0.12	0.07	0.14	0.11	0.21	0.18	0.27	0.21
h	13	0.16	0.16	0.11	0.14	0.10	0.11	0.15	0.16	0.10	0.13	0.31	0.20
i	15	0.14	0.10	0.11	0.12	0.09	0.05	0.15	0.14	0.17	0.12	0.19	0.17
j	17	0.18	0.12	0.11	0.12	0.05	0.04	0.13	0.11	0.08	0.11	0.17	0.14
k	19	0.14	0.09	0.12	0.08	0.09	0.04	0.08	0.09	0.12	0.15	0.18	0.15
l	21	0.10	0.07	0.13	0.04	0.11	0.06	0.06	0.08	0.09	0.12	0.15	0.11

θ is the included angle between the loading direction and the x-direction
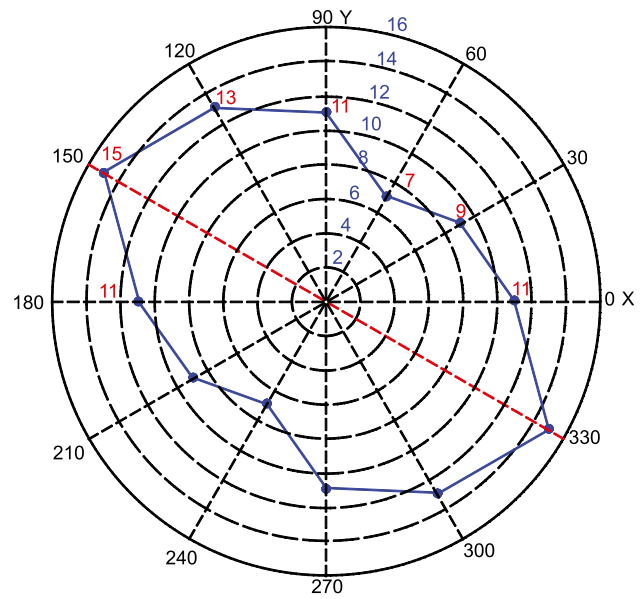

Fig. 12 Anisotropy of the REV size (unit: m)

area per unit volume (P_{32}) (Dershowitz [1984](); Einstein and Locsin [2012]()), was used to determine the geometrical REV. As shown in Fig. [14]()a, the values of P_{30} for rock samples in different regions change dramatically when the sample size varies from 0.05 to 3 m, but converge to a value of 0.26 m^{-3} when the sample size is larger than 5 m. Figure [14]()b shows that the values of P_{32} converge to a value of 1.60 m^{-1} when the sample size is close to 21 m. As listed in Table [8](), the C_V values of P_{30} and are P_{32} less than 0.2 when the sample size reaches 5 m and 7 m, respectively. Therefore, the P_{30}-based and P_{32}-based REV sizes are 5 m and 7 m, respectively. Compared with P_{30}, P_{32} yields a larger REV size. This could be attributed to that P_{32} reflects the influence of fracture length and density, whereas P_{30} only reflects the influence of fracture density. Based on P_{30} and P_{32}, the geometrical REV size is estimated to be 7 m.

An interesting phenomenon was observed that the geometrical REV size is equal to the UCS-based and E-based REV size with $\theta=60°$ which is the minimum in the six loading directions. It seems that the geometrical REV defines the lower bound of the REV size of the rock mass. However, geometrical parameters cannot reflect the anisotropy of the mechanical properties of rock masses. Besides, the mechanical properties of rock masses are affected by many properties of fractures such as fracture size, orientation, connectivity, infilling, and density. The REV size obtained by geometrical parameters may lead to an incorrect characterization and property upscaling.
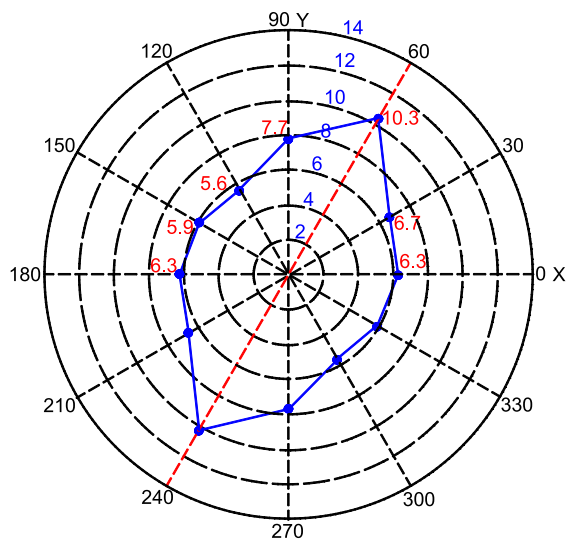
(a) UCS (unit: MPa)
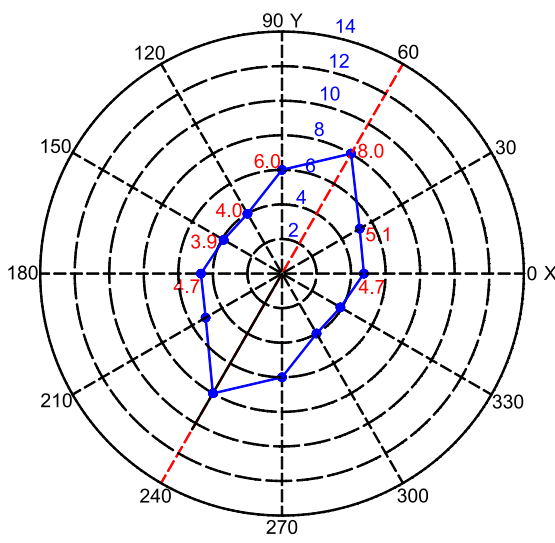
(b) E (unit: GPa)

**Fig. 13** Anisotropy of **a** UCS and **b** E for rock samples in a REV size

Discussion

Note that uncertainty exists in the simulations due to the random distribution of joints in the model. To reduce the uncertainty, five DFN models were selected from different regions of the "master" DFN model. In the simulations using PFC3D, even if some fractures go beyond the size of the model, the model can be loaded normally. The part of a fracture within the model will be considered in the calculation, whereas the part outside the model will not be considered.

However, when extracting the DFN model from the "master" DFN model, if the centroid of a joint is not within the model, the joint will be deleted, which will inevitably cause uncertainty in the simulations. To solve this problem, when establishing the SRM models using the DFN models, the largest BPM model is set as 21 m × 21 m × 42 m, but the size of the DFN models is fixed at 27 m × 27 m × 54 m. Therefore, a joint cannot be deleted unless its radius is larger than 6 m and its centroid is out of the range of 27 m × 27 m × 54 m. We checked the "master" DFN model with the size of 100 m × 60 m × 60 m, and the percentage of fractures with a radius larger than 6 m is less than 0.09% of all fractures. Thus, the influence of the censoring effect on the results could be eliminated by this method.

The simulation results suggest that jointed rock mass displays significant anisotropy in uniaxial compression tests, and the REV size varies with rotational angle and displays obvious anisotropy and directionality. According to Fig. 12, the REV size for $\theta = 60°$ is the minimum, whereas the REV size for $\theta = 150°$ is the maximum. The stress–strain curves for the two loading directions were selected to make a comparative study, as shown in Fig. 15. The mechanical properties of rock mass samples for $\theta = 150°$ are lower than those for $\theta = 60°$ when the model size is smaller than the REV size. However, when the model size is larger than the REV size (i.e., 15 m), the difference in mechanical properties for the two loading directions is relatively small.

**Fig. 14** Variation of the values of **a** P_{30} and **b** P_{32} with rock sample sizes
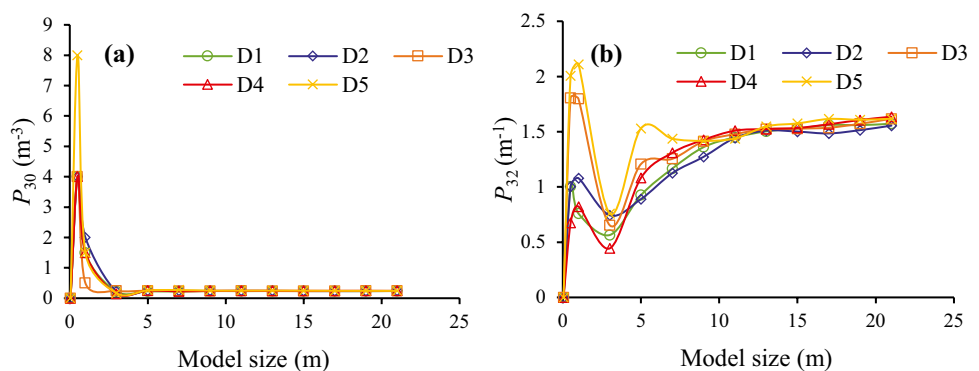
Table 8 CV results for estimating REV size based on fracture intensity

Sample ID	Sample size (m)	CV of P_{30}	CV of P_{32}
a	0.5	0	0.44
b	1	0.39	0.46
c	3	0.21	0.21
d	5	0.05	0.23
e	7	0.08	0.10
f	9	0.02	0.05
g	11	0.02	0.02
h	13	0.03	0.01
i	15	0.03	0.02
j	17	0.02	0.03
k	19	0.02	0.02
l	21	0.01	0.02

Conclusions

This paper presents an investigation on the scale dependency and anisotropy of mechanical properties of a jointed rock mass. A three-dimensional (3D) discrete fracture network (DFN) model was built based on joint data collected from an exploration tunnel at a dam site in southwest China. The model was validated and subsequently sampled to procure 455 rectangular samples with a constant height-to-width ratio of 2 and width varying from 0.05 to 21 m. The samples were introduced into a 3D particle flow code (PFC3D) model to create synthetic rock mass (SRM) samples. Numerical uniaxial compressive tests with different loading directions were conducted to obtain the variations of the values of UCS and elastic modulus with sample sizes.

Fig. 15 Comparison of stress–strain graphs at different scales and orientations
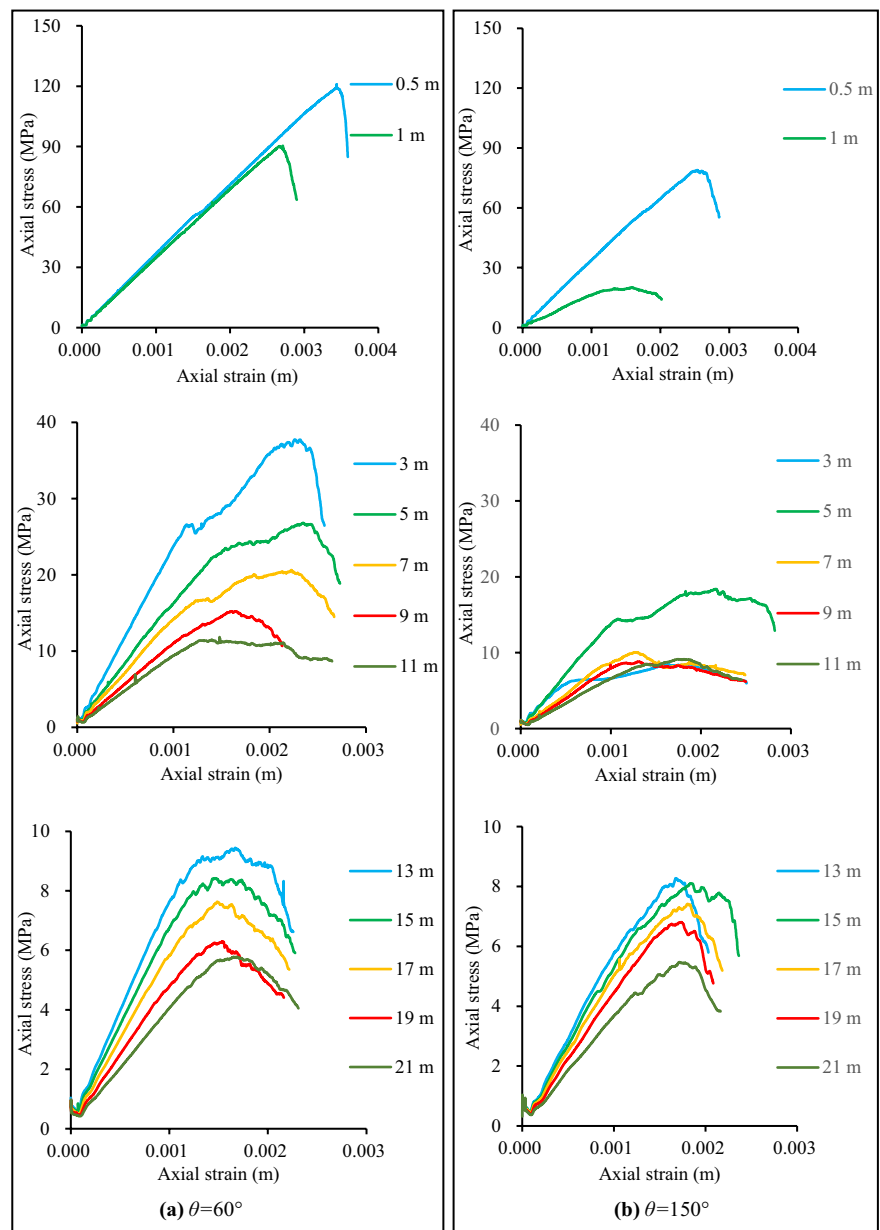
It is determined that the mechanical REV size in the vertical direction is 19 m based on the UCS-based and E-based indicators. The values of UCS and E in the REV size are 8.8 MPa and 5.0 GPa, respectively. Compared with the values of UCS and E of intact rock, the values of UCS and E of the rock mass in the vertical direction are relatively decreased by 93.1% and 87.1%, respectively. In the horizontal plane, the mechanical REV sizes in different directions vary from 7 to 15 m. The mechanical properties of rock mass samples in a REV size exhibit strong anisotropy, with the values of UCS and E changing from 5.9 to 10.3 MPa and 3.9 to 8.0 GPa, respectively. The mechanical properties of rock mass samples for $\theta = 60°$ is the maximum, but the REV size in this direction is the minimum. Besides, the mechanical properties of rock mass samples for $\theta = 150°$ is the minimum, whereas the REV size in this direction is the maximum. Therefore, it could be concluded that the REV size has a negative relationship with the mechanical properties of the rock mass. The volumetric fracture intensity was used to determine the geometrical REV for comparison. The geometrical REV size was estimated to be 7 m, equal to the minimum of the mechanical REV size, indicating that the geometrical REV defines the lower bound of the REV size of the rock mass.

However, the parallel bond model suffers from an overestimation of tensile strength and an underestimation of the failure envelope. To solve this problem, a flat-joint model was proposed by Potyondy (2012), which can reproduce the mechanical behavior of a material under different loading conditions (Potyondy 2015; Bahaaddini et al. 2021). It is recommended that the flat-joint model could be used to study the mechanical behaviors of jointed rock masses in future studies.

Data availability All data used to support the findings of this study are included within the article, and there are not any restrictions on data access.

Declarations

Conflict of interest The authors declare no competing interests.

References

Azizmohammadi S, Matthäi SK (2017) Is the permeability of naturally fractured rocks scale dependent? Water Resour Res 53(9):8041–8063

Baghbanan A (2008) Scale and stress effects on hydro-mechanical properties of fractured rock masses. PhD dissertation, Royal Institute of Technology (KTH), Stockholm, Sweden

Bahaaddini M, Hagan PC, Mitra R, Hebblewhite BK (2015) Parametric study of smooth joint parameters on the shear behaviour of rock joints. Rock Mech Rock Eng 48(3):923–940

Bahaaddini M, Hagan PC, Mitra R, Khosravi MH (2016) Experimental and numerical study of asperity degradation in the direct shear test. Eng Geol 204:41–52

Bahaaddini M, Sharrock G, Hebblewhite BK (2013) Numerical direct shear tests to model the shear behaviour of rock joints. Comput Geotech 51:101–115

Bahaaddini M, Sheikhpourkhani AM, Mansouri H (2021) Flat-joint model to reproduce the mechanical behaviour of intact rocks. Eur J Environ Civ Eng 25:1427–1448

Bastola S, Cai M, Damjanac B (2020) Slope stability assessment of an open pit using lattice-spring-based synthetic rock mass (LS-SRM) modeling approach. J Rock Mech Geotech Eng 13:275–288

Bear J (1972) Dynamics of fluids in porous media. Soil Sci 10(2):162–163

Bieniawski Z (1968) Propagation of brittle fracture in rock. In: The 10th US symposium on rock mechanics, Texas, pp 409

Bieniawski ZT (1973) Engineering classification of jointed rock masses. Civ Eng S Afr 15:335–343

Chen JP, Xiao SF, Wang Q (1995) Three dimensional network modeling of stochastic fractures. Northeast Normal University Press, Changchun, China

Chen SH, Feng XM, Isam S (2008) Numerical estimation of REV and permeability tensor for fractured rock masses by composite element method. Int J Numer Anal Methods Geomech 32(12):1459–1477

Cho JW, Kim H, Jeon S, Min KB (2012) Deformation and strength anisotropy of Asan gneiss, Boryeong shale, and Yeoncheon schist. Int J Rock Mech Min Sci 50:158–169

Dershowitz WS (1984) Rock joint systems. PhD dissertation, Massachusetts Institute of Technology, Cambridge

Einstein HH, Locsin J (2012) Modeling rock fracture intersections and application to the Boston area. J Geotech Geoenviron 138(11):1415–1421

Esmaieli K, Hadjigeorgiou J, Grenon M (2010) Estimating geometrical and mechanical REV based on synthetic rock mass models at Brunswick Mine. Int J Rock Mech Min Sci 47(6):915–926

Hammah RE, Curran JH (1999) On distance measures for the fuzzy K-means algorithm for joint data. Rock Mech Rock Eng 32:1–27

Han X, Chen J, Wang Q, Li Y, Zhang W, Yu T (2016) A 3D fracture network model for the undisturbed rock mass at the Songta dam site based on small samples. Rock Mech Rock Eng 49(2):611–619

Hardebol NJ, Maier C, Nick H, Geiger S, Bertotti G, Boro H (2015) Multiscale fracture network characterization and impact on flow: a case study on the latemar carbonate platform. J Geophys Res-Sol Ea 120(12):8197–8222

Hoek E, Brown ET (1997) Practical estimates of rock mass strength. Int J Rock Mech Min Sci 34(8):1165–1186

Huang H, Shen J, Chen Q, Karakus M (2020) Estimation of REV for fractured rock masses based on geological strength index. Int J Rock Mech Min Sci 126:104179

Hudson JA, Harrison JP (1997) Engineering rock mechanics: an introduction to the principles. Elsevier Science, Amsterdam, Netherlands

Ivars DM, Pierce ME, Darcel C, Reyes-Montes J, Potyondy DO, Young RP, Cundall PA (2011) The synthetic rock mass approach for jointed rock mass modelling. Int J Rock Mech Min 48(2):219–244

Ivars DM, Potyondy D, Pierce M, Cundall P (2008) The smooth-joint contact model. In: Proceedings of the 8th World Congress on Computational Mechanics, Barcelona, Italy, pp 2735–2742

Khani A, Baghbanan A, Hashemolhosseini H (2013) Numerical investigation of the effect of fracture intensity on deformability

and REV of fractured rock masses. Int J Rock Mech Min Sci 63:104–112

Kulatilake PHSW, Panda BB (2000) Effect of block size and joint geometry on jointed rock hydraulics and REV. J Eng Mech 126(8):850–858

Kulatilake PHSW, Um J, Wang M, Escandon RF, Narvaiz J (2003) Stochastic fracture geometry modeling in 3-D including validations for a part of arrowhead east tunnel, California, USA. Eng Geol 70:131–155

Kulatilake PHSW, Wathugala DN, Stephansson OVE (1993) Stochastic three dimensional joint size, intensity and system modelling and a validation to an area in Stripa Mine. Sweden Soils Found 33(1):55–70

Laghaei M, Baghbanan A, Hashemolhosseini H, Dehghanipoodeh M (2018) Numerical determination of deformability and strength of 3D fractured rock mass. Int J Rock Mech Min Sci 110:246–256

Lang PS, Paluszny A, Zimmerman RW (2014) Permeability tensor of three-dimensional fractured porous rock and a comparison to tracemap predictions. J Geophys Res Solid Earth 119(8):6288–6307

Li Y, Chen J, Shang Y (2017) Connectivity of three-dimensional fracture networks: a case study from a dam site in southwest China. Rock Mech Rock Eng 50(1):241–249

Li Y, Chen J, Shang Y (2018) Determination of the geometrical REV based on fracture connectivity: a case study of an underground excavation at the Songta dam site. China Bull Eng Geol Environ 77(4):1599–1606

Li Y, Wang Q, Chen J, Han L, Song S (2014) Identification of structural domain boundaries at the Songta dam site based on nonparametric tests. Int J Rock Mech Min Sci 70:177–184

Long JCS, Remer JS, Wilson CR, Witherspoon PA (1982) Porous media equivalents for networks of discontinuous fractures. Water Resour Res 18(3):645–658

Lyu W, Zhang L, Yang B, Chen Y (2021) Analysis of stability of the Baihetan arch dam based on the comprehensive method. Bull Eng Geol Environ 80(2):1219–1232

Manda AK, Mabee SB (2010) Comparison of three fracture sampling methods for layered rocks. Int J Rock Mech Min Sci 47(2):218–226

Marinos P, Hoek E (2000) GSI: a geologically friendly tool for rock mass strength estimation. In: Proceedings of the International Conference on Geotechnical and Geological Engineering, Lancaster, pp1422–1446

Mauldon M, Dunne WM, Rohrbaugh MB (2001) Circular scanlines and circular windows: new tools for characterizing the geometry of fracture traces. J Struct Geol 23(2):247–258

Mehranpour MH, Kulatilake PHSW (2017) Improvements for the smooth joint contact model of the particle flow code and its applications. Comput Geotech 87:163–177

Min KB, Jing L (2003) Numerical determination of the equivalent elastic compliance tensor for fractured rock masses using the distinct element method. Int J Rock Mech Min Sci 40(6):795–816

Min KB, Jing L, Stephansson O (2004) Determining the equivalent permeability tensor for fractured rock masses using a stochastic REV approach: method and application to the field data from sellafield. UK Hydrogeol J 12(5):497–510

Ni P, Wang S, Wang C, Zhang S (2017) Estimation of REV size for fractured rock mass based on damage coefficient. Rock Mech Rock Eng 50(3):555–570

Oda M (1982) Fabric tensor for discontinuous geological materials. Soils Found 22(4):96–108

Oda M (1983) A method for evaluating the effect of crack geometry on the mechanical behavior of cracked rock masses. Mech Mater 2(2):163–171

Oda M (1988) A method for evaluating the representative elementary volume based on joint survey of rock masses. Can Geotech J 25(3):440–447

Pariseau WG, Puri S, Schmelter SC (2008) A new model for effects of impersistent joint sets on rock slope stability. Int J Rock Mech Min Sci 45:122–131

Park B, Min KB (2015) Bonded-particle discrete element modeling of mechanical behavior of transversely isotropic rock. Int J Rock Mech Min Sci 76:243–255

Potyondy D, Cundall P (2004) A bonded-particle model for rock. Int J Rock Mech Min Sci 41(8):1329–1364

Potyondy DO (2012) A flat-jointed bonded-particle material for hard rock. In: Proceedings of the 46th US Rock Mechanics/Geomechanics Symposium, Chicago, pp 24–27

Potyondy DO (2015) The bonded-particle model as a tool for rock mechanics research and application: current trends and future directions. Geosystem Eng 18:1–28

Wang M, Kulatilake PHSW, Um J, Narvaiz J (2002) Estimation of REV size and three-dimensional hydraulic conductivity tensor for a fractured rock mass through a single well packer test and discrete fracture fluid flow modeling. Int J Rock Mech Min Sci 39(7):887–904

Wang P, Ren F, Miao S, Cai M, Yang T (2017) Evaluation of the anisotropy and directionality of a jointed rock mass under numerical direct shear tests. Eng Geol 225:29–41

Warburton PM (1980) A stereological interpretation of joint trace data. Int J Rock Mech Min Sci Geomech Abstr 17:181–190

Wu H, Pollard D (1995) An experimental study of the relationship between joint spacing and layer thickness. J Struct Geol 17(6):887–905

Wu N, Liang ZZ, Li YC, Li H, Li WR, Zhang ML (2019) Stress-dependent anisotropy index of strength and deformability of jointed rock mass: insights from a numerical study. Bull Eng Geol Environ 78:5905–5917

Wu Q, Jiang Y, Tang H, Luo H, Wang X, Kang J, Zhang S, Yi X, Fan L (2020) Experimental and numerical studies on the evolution of shear behaviour and damage of natural discontinuities at the interface between different rock types. Rock Mech Rock Eng 53:3721–3744

Wu Q, Kulatilake PHSW (2012) REV and its properties on fracture system and mechanical properties, and an orthotropic constitutive model for a jointed rock mass in a dam site in China. Comput Geotech 43:124–142

Xia L, Zheng Y, Yu Q (2016) Estimation of the REV size for blockiness of fractured rock masses. Comput Geotech 76:83–92

Zhang L, Einstein HH (1998) Estimating the mean trace length of rock discontinuities. Rock Mech Rock Eng 31(4):217–235

Zhang L, Einstein HH (2000) Estimating the intensity of rock discontinuities. Int J Rock Mech Min Sci 37(5):819–837

Zhang W, Chen JP, Liu C, Huang R, Li M, Zhang Y (2012) Determination of geometrical and structural representative volume elements at the Baihetan dam site. Rock Mech Rock Eng 45(3):409–419

Zhang Y, Stead D, Elmo D (2015) Characterization of strength and damage of hard rock pillars using a synthetic rock mass method. Comput Geotech 65:56–72

Zhao WH, Huang RQ (2018) Potential failure paths of fractured rock slope based on synthetic rock mass (SRM) method. Chin J Rock Mech Eng 37(8):1843–1855

Zheng J, Wang X, Lu Q, Sun H, Guo J (2020) A new determination method for the permeability tensor of fractured rock masses. J Hydro 585:124811

Zou L, Xu W, Meng G, Ning Y, Wang H (2018) Permeability anisotropy of columnar jointed rock masses. KSCE J Civ Eng 22(10):3802–3809